# Linearized Double-Shock Approximate Riemann Solver for Augmented Linear Elastic Solid

Zhiqiang Zeng, Chengliang Feng, Changsheng Yu
and Tiegang Liu*

*LMIB and School of Mathematical Sciences, Beihang University,
Beijing 100191, China*

**Abstract.** In this work, in order to capture discontinuities correctly in linear elastic solid, augmented internal energy is defined according to the first law of thermodynamics and Hooke's law. The non-conservative linear elastic system is then rewritten into a conservative form with the help of an augmented total energy equation. We find that the non-physical oscillations occur to the popular HLL and HLLC approximate Riemann solvers when directly applied to simulate the augmented linear elastic solid. We analyze the intrinsic reason by defining a discrepancy factor which can be used to estimate the difference of the total stress across a contact discontinuity, where it is physically required to be continuous. We discover that non-physical oscillations inevitably appear in the vicinity of the contact discontinuity if this factor is away from zero for an approximate Riemann problem solver. In order to overcome this difficulty, we propose an approximate Riemann solver based on the linearized double-shock technique. Theoretical analysis and numerical results show that in comparison to the HLL and HLLC approximate Riemann solvers, the present linearized double-shock Riemann solver can eliminate the non-physical oscillations effectively.

**AMS subject classifications**: 52B10, 65D18, 68U05, 68U07

**Key words**: Linear elastic solid, approximate Riemann solver, discrepancy factor.

## 1. Introduction

In recent decades, various elastic and plastic models, such as hyper-elastic plastic models and hypo-elastic plastic models, have been developed for simulating mechanical behaviors of solid materials. To better understand the performance of those theoretical models, researchers [9–11,20,21] have put much effort into developing exact solutions concerning various models. Those exact solutions are precious and have played an important role in constructing and verifying numerical solvers in the simulation of

---

*Corresponding author. *Email address:* `liutg@buaa.edu.cn` (T. Liu)

compressible solids. In this work, we focus on developing numerical method for linear elastic solid and verifying it with exact solutions.

A hyper-elastic plastic model usually satisfies the second law of thermodynamics and the corresponding governing system can be written in a conservative form. Garaizar [11] proposed an exact iterative Riemann problem solver for the isotropic hyper-elastic model. Based on the above work, LeFloch and Olsson [15] presented an approximate Riemann solver, which only utilized features of shock waves. Gavrilyuk *et al.* [12] constructed an approximate Riemann solver for the non-conservative non-linear elastic system. Miller [20] presented an exact iterative Riemann solver for the general hyper-elastic system. Barton *et al.* [1] presented another iterative method for finding the exact solution to the Riemann problem with non-linear elasticity. Trangenstein *et al.* [22] constructed an approximate Riemann solver for considering the interaction of elastic waves at cell boundaries.

Compared with hyper-elastic plastic models, a hypo-elastic plastic model might be inconsistent with thermodynamics strictly and often results in a non-conservation governing system. However, such a model bears the advantages of reproducing experimental data accurately (especially for metal materials), introducing plastic deformation naturally, and dealing with complex multi-dimensional boundary problems easily. For a hypo-elastic plastic model, an equation of state (EOS) or Hooke's law is usually applied in the elastic region, the EOS commonly includes the Murnagham equation of state and the Mie-Gruüneisen equation of state. The former is suitable for simulating the solid state at high temperature and high pressure. Tang *et al.* [21] put forward an exact Riemann solver for the hydro-elastoplastic solid. For the latter, Maire *et al.* [19] proposed a nodal-based Riemann solver in the lagrangian coordinate. Chen *et al.* [2] proposed an approximate iterative solver for elastic-plastic Riemann problems. Cheng and colleges [3, 4] developed a two-rarefaction Riemann solver (TRRSE) and Harten-Lax-van Leer-contact (HLLC) approximate Riemann solvers for elastic waves. In their work [3], they found the popular HLLC approximate Riemann solver suffered numerical oscillations. Later, they proposed a multi-material HLLC with both elastic and plastic (MHLLCEP) approximate Riemann solvers [17] to fix the above difficulty by enforcing the continuity of total stress across the contact discontinuity. Recently, Li *et al.* [16] presented another HLLC-type approximate Riemann solver, where the elastic-plastic shear wave was considered, to overcome the above-mentioned problem.

In practice, for metal materials under not very high temperature and pressure, Hooke's law is more appropriate in reflecting the mechanical behavior of metals. This usually leads to linear elastic modeling to the solid. Wilkins [23] extensively investigated the linear elastic model, in which Hooke's law was applied to model the elastic region, and perfect plasticity was adopted to treat the plastic region with an equation of state. As a result, the governing system is non-conservative in the elastic region, while it is conservative in the plastic region. When there is a shock wave in the elastic region, a non-conservation system might lead to incorrect numerical results as found by Gavrilyuk *et al.* [12]. Barton *et al.* [1] and Trangenstein *et al.* [22] also pointed out that the non-conservative system of an elastic model produced non-physical character-

istic speeds. Consequently, the maintenance of conservation is essential to deal with weak solutions (shock and contact waves) for elastic solids. To capture the shock wave correctly with Hooke's law, Gao *et al.* [9, 10] constructed self-consistent conservation equations of mass and momentum by substituting the integral form of Hooke's law into the momentum equation. Based on that, they gave all the possible exact solutions for the linear elastic-perfectly plastic Riemann problem [10] and proposed a non-iterative solution structure-based adaptive approximate (SSAA) Riemann solver for simulating the elastic-perfectly plastic flows in solid [9].

In the work [9], the governing system with the perfect plastic model is conservative and contains a conserved energy equation, while the governing system in the elastic region is non-conservative without any energy equation. As a result, the coupling of a conservation system with a non-conservation system makes the production of plastic energy unnatural during the transition of the elastic state to the plastic state. For tackling this problem, it is necessary to restore the energy conservation equation in the linear elastic region. In this work, we will define augmented specific internal energy by utilizing the first law of thermodynamics and Hooke's law, and the conserved total energy equation can then be put back into the governing system. Such augmented technology has been employed by Liu [18] for modeling compressible water with the Tait equation.

For the conservation system with the augmented total energy equation, we will show that non-physical oscillations occur to the popular Harten-Lax-van Leer (HLL) [6–8, 14] and Harten-Lax-van Leer-contact (HLLC) [13] approximate Riemann solvers when they are directly applied. We shall theoretically analyze the defects of HLL and HLLC approximate Riemann solvers by using a discrepancy factor which is defined based on a physical requirement that the total stress should be continuous across a contact wave. In order to correct the defects of the above solvers, we shall propose an approximate Riemann solver based on the linearized double-shock technique [5] for the augmented system.

This paper is organized as follows. In Section 2, we develop the conserved system for the linear elastic solid with the augmented total energy equation, and the compatibility between the augmented system and the original system is analyzed. The exact Riemann solver for the Riemann problem of the linear elastic system is presented in Section 3. In Sections 4 and 5, the discrepancy of total stress to the HLL and HLLC Riemann solvers are analyzed, respectively. In Section 6, we propose a linearized double-shock approximate Riemann solver. Several numerical examples are presented in Section 7 to validate the method. Finally, conclusions are given in Section 8.

## 2. Governing equations

### 2.1. Non-conservative equations

For the one-dimensional linear elastic solid, the non-conservative governing equations are as follows [10]:

$$\frac{\partial U}{\partial t} + \frac{\partial F(U)}{\partial x} = \mathbf{S}(U), \tag{2.1}$$

where

$$U = \begin{bmatrix} \rho \\ \rho u \\ \rho \sigma_x \end{bmatrix}, \quad F(U) = \begin{bmatrix} \rho u \\ \rho u^2 - \sigma_x \\ \rho u \sigma_x \end{bmatrix}, \quad \mathbf{S}(U) = \begin{bmatrix} 0 \\ 0 \\ -\left(K + \frac{4}{3}\mu\right)\dot{\rho} \end{bmatrix}. \tag{2.2}$$

Here, $\rho$ is the density, $u$ is the velocity, $\sigma_x$ is the total stress, $K$ is the bulk modulus and $\mu$ is the shear modulus. The total stress $\sigma_x$ can be decomposed into the hydrostatic pressure $p$ and the deviatoric stress $s_x$, which is

$$\sigma_x = -p + s_x. \tag{2.3}$$

With Hooke's law, we have

$$\dot{p} = K\frac{\dot{\rho}}{\rho}, \quad \dot{s}_x = 2\mu \left( \dot{\varepsilon}_x + \frac{1}{3}\frac{\dot{\rho}}{\rho} \right). \tag{2.4}$$

Here, the variable $\varepsilon_x$ is the strain. The dot "·" represents the derivative of a physical quantity in the Lagrangian coordinate.

## 2.2. Augmented equations

In this section, augmented specific internal energy $e$ is constructed for the linear elastic governing equations by utilizing Hooke's law and the first law of thermodynamics. Integrating (2.4), we obtain

$$\rho = \rho_0 \exp\left(\frac{p - p_0}{K}\right), \tag{2.5}$$

where $\rho_0$ is the density at a reference pressure $p_0$. Supposing the solid is adiabatic, the first law of thermodynamics goes to

$$de + pd\left(\frac{1}{\rho}\right) = 0. \tag{2.6}$$

Substituting (2.5) into (2.6) yields

$$de + pd\left(\frac{1}{\rho_0 \exp\left(\frac{p-p_0}{K}\right)}\right) = 0. \tag{2.7}$$

Integrating the above equation, we can get

$$p = \rho e_0 - \rho e - K, \tag{2.8}$$

where the $e$ serves to be the specific internal energy, $e_0$ is a given constant which guarantees positive pressure. Hence, we can define augmented total energy $E$ as follows:

$$E = \rho e + \frac{1}{2}\rho u^2. \tag{2.9}$$

The system (2.1) can then be rewritten as

$$\frac{\partial U}{\partial t} + \frac{\partial G(U)}{\partial x} = 0, \tag{2.10}$$

where

$$U = \begin{bmatrix} \rho \\ \rho u \\ E \end{bmatrix}, \quad G(U) = \begin{bmatrix} \rho u \\ \rho u^2 - \sigma_x \\ (E - \sigma_x) u \end{bmatrix} \tag{2.11}$$

with the constitutive model as

> (I)   Total stress decomposition: $\sigma_x = -p + s_x$,
>
> (II)  Hooke's law: $\dot{s}_x = 2\mu\left(\dot{\varepsilon}_x + \frac{1}{3}\frac{\dot{\rho}}{\rho}\right)$,
>
> (III) Augmented equation of state:            (2.12)
>
> $p(\rho, e) = \rho e_0 - \rho e - K, E = \rho e + \frac{1}{2}\rho u^2$,
>
> (IV)  Minimized hydrostatic pressure: $\min p = -\frac{1}{3}Y_0$,

where $Y_0$ is the yield strength of the material in simple tension.

## 2.3. Compatibility analysis

### 2.3.1. Non-conservative form

For the quasi-linear form of governing system (2.1)-(2.2), the Riemann problem under the Eulerian framework is described as

$$\frac{\partial W}{\partial t} + A(W)\frac{\partial W}{\partial x} = 0,$$

$$W|_{t=0} = \begin{cases} W_L|_{t=0}, & x < x_0, \\ W_R|_{t=0}, & x > x_0, \end{cases} \tag{2.13}$$

where

$$A(W) = \begin{bmatrix} u & \rho & 0 \\ 0 & u & 1/\rho \\ 0 & -K - 4\mu/3 & u \end{bmatrix}. \tag{2.14}$$

Here, $x_0$ is the initial discontinuity position, $W = (\rho, u, \sigma_x)^T$, $W_L = (\rho_L, u_L, \sigma_{xL})^T$ and $W_R = (\rho_R, u_R, \sigma_{xR})^T$ are the initial primitive constant variables of the linear elastic solid at time $t = 0$.

The eigenvalues and corresponding right eigenvectors of the Jacobian matrix $A(W)$ are

$$\lambda_1 = u - c, \quad \lambda_2 = u, \quad \lambda_3 = u + c, \tag{2.15}$$

and

$$\mathbf{R}_1 = \begin{bmatrix} -\rho \\ c \\ -K - 4\mu/3 \end{bmatrix}, \quad \mathbf{R}_2 = \begin{bmatrix} 1 \\ 0 \\ 0 \end{bmatrix}, \quad \mathbf{R}_3 = \begin{bmatrix} \rho \\ c \\ K + 4\mu/3 \end{bmatrix}, \tag{2.16}$$

where $c = \sqrt{(4\mu + 3K)/(3\rho)}$.

It is easy to show that $\lambda_2$-field is linearly degenerated, $\lambda_1$-field and $\lambda_3$-field are genuinely non-linear. The Riemann invariants for the respective $\lambda_1$-field and $\lambda_3$-field are given by

$$\frac{\mathrm{d}\rho}{\pm\rho} = \frac{\mathrm{d}\rho u}{\pm c} = \frac{\mathrm{d}\sigma_x}{\pm(K + 4\mu/3)}. \tag{2.17}$$

According to above ODEs, we can get

$$I_{\lambda_1}(\rho, u) = u - \sqrt{\frac{16\mu + 12K}{3\rho}} = \text{ constant},$$

$$I_{\lambda_1}(\rho, \sigma_x) = \sigma_x + \left(\frac{4\mu}{3} + K\right)\ln\rho = \text{ constant}, \tag{2.18}$$

$$I_{\lambda_3}(\rho, u) = u + \sqrt{\frac{16\mu + 12K}{3\rho}} = \text{ constant},$$

$$I_{\lambda_3}(\rho, \sigma_x) = \sigma_x + \left(\frac{4\mu}{3} + K\right)\ln\rho = \text{ constant}. \tag{2.19}$$

For $\lambda_2$-field, the Riemann invariants are obtained as

$$\frac{\mathrm{d}\rho}{1} = \frac{\mathrm{d}\rho u}{0} = \frac{\mathrm{d}\sigma_x}{0}. \tag{2.20}$$

By solving (2.20), one can obtain

$$I_{\lambda_2}(\rho, u) = u = \text{ constant},$$
$$I_{\lambda_2}(\rho, \sigma_x) = \sigma_x = \text{ constant}. \tag{2.21}$$

The expression of (2.21) implies that the velocity and total stress are continuous across the $\lambda_2$-field. Thus, $\lambda_2$-field is a contact discontinuity.

## 2.3.2. Conservative form

According to (2.5) and (2.8), only one variable is independent of each other among $p, e, \rho$. Assuming this independent variable is $\rho$, we can get

$$f(\rho) := \sigma_x = -p + s_x = -\left(K + \frac{4\mu}{3}\right)\ln\rho + C, \quad g = -\frac{\partial f}{\partial\rho}, \tag{2.22}$$

where $C$ is an arbitrary constant. Substituting (2.22) into (2.11), let $m = \rho, n = \rho u, l = E$, we can write the augmented governing system (2.10)-(2.11) into its quasi-linear form

$$\frac{\partial U}{\partial t} + B(U) \frac{\partial U}{\partial x} = 0, \tag{2.23}$$

where

$$B = \begin{bmatrix} 0 & 1 & 0 \\ -\dfrac{n^2}{m^2} - g & \dfrac{2n}{m} & 0 \\ -\dfrac{nl}{x^2} - n\dfrac{mg - f}{m^2} & \dfrac{l - f}{m} & \dfrac{n}{m} \end{bmatrix}. \tag{2.24}$$

Here, $U$ is a vector of conservative variables $(m, n, l)^T$. We can obtain its three eigenvalues

$$\gamma_1 = \frac{n - \sqrt{g}m}{m} = u - c, \quad \gamma_2 = \frac{n}{m} = u, \quad \gamma_3 = \frac{n + \sqrt{g}m}{m} = u + c, \tag{2.25}$$

and corresponding right eigenvector matrix

$$R = \begin{bmatrix} 0 & -\dfrac{m}{f + \sqrt{g}n - l} & \dfrac{m}{-f + \sqrt{g}n + l} \\ 0 & -\dfrac{n - \sqrt{g}m}{f + \sqrt{g}n - l} & -\dfrac{(-\sqrt{g})m - n}{-f + \sqrt{g}n + l} \\ 1 & 1 & 1 \end{bmatrix}. \tag{2.26}$$

We can show that the $\gamma_1$-field and $\gamma_3$-field are genuinely non-linear for the conservative system, while the $\gamma_2$-field is linearly degenerated. For the $\gamma_1$-field, the Riemann invariants can be calculated by

$$\frac{\mathrm{d}m}{-\frac{m}{f + \sqrt{g}n - l}} = \frac{\mathrm{d}n}{-\frac{n - \sqrt{g}m}{f + \sqrt{g}n - l}} = \frac{\mathrm{d}l}{1}. \tag{2.27}$$

The augmented energy $l$ is completely determined by density $m$ and velocity $n/m$, only one ordinary differential equation is obtained in the (2.27), which is

$$\frac{\mathrm{d}m}{-\frac{m}{f + \sqrt{g}n - l}} = \frac{\mathrm{d}n}{-\frac{n - \sqrt{g}m}{f + \sqrt{g}n - l}}. \tag{2.28}$$

Thus the Riemann invariant for $\gamma_1$-field can be given by

$$I_{\gamma_1}(m, n) = \frac{n}{m} - \sqrt{\frac{16\mu + 12K}{3m}} = u - \sqrt{\frac{16\mu + 12K}{3\rho}} = \text{ constant.} \tag{2.29}$$

Similarly, the Riemann invariant for $\gamma_3$-field can be obtained by

$$I_{\gamma_3}(m, n) = \frac{n}{m} + \sqrt{\frac{16\mu + 12K}{3m}} = u + \sqrt{\frac{16\mu + 12K}{3\rho}} = \text{ constant.} \tag{2.30}$$

Hooke's law still holds for the $\gamma_1$-field and $\gamma_3$-field, we can get

$$
\begin{aligned}
I_{\gamma_1}(m, \sigma_x) = I_{\gamma_3}(m, \sigma_x) &= \sigma_x + \left( \frac{4\mu}{3} + K \right) \ln m \\
&= \sigma_x + \left( \frac{4\mu}{3} + K \right) \ln \rho = \text{ constant.} \qquad (2.31)
\end{aligned}
$$

For the $\gamma_2$-field, according to (2.22), we can prove that $f(m)$ is a monotone and continuous function. The inverse function for $f(m)$ can be given by

$$
\phi(\sigma_x) := m = C_0 \exp\left( -\frac{\sigma_x}{\frac{4}{3}\mu + K} \right), \qquad (2.32)
$$

where $C_0$ is a constant. Combining (2.26) with (2.32), the Riemann invariants of the $\gamma_2$-field can be obtained by solving the following ODEs:

$$
\frac{\mathrm{d}\phi(\sigma_x)}{0} = \frac{\mathrm{d}n}{0} = \frac{\mathrm{d}l}{1}. \qquad (2.33)
$$

The corresponding Riemann invariants are

$$
\begin{aligned}
I_{\gamma_2}(m, n) &= \frac{n}{m} = u = \text{ constant,} \\
I_{\gamma_2}(m, \sigma_x) &= \sigma_x = \text{ constant.}
\end{aligned} \qquad (2.34)
$$

As a result, the $\gamma_2$-field is a contact discontinuity, across which the velocity and the total stress are continuous. Comparing (2.15) with (2.25) and (2.17)-(2.21) with (2.27)-(2.34), we can conclude the following conclusion.

**Theorem 2.1.** *The eigenvalues systems and corresponding Riemann invariants of the augmented conservative system* (2.23)-(2.24) *and non-conservative system* (2.1)-(2.2) *are consistent.*

## 3. Exact Riemann solver

For linear elastic solid, the one-dimensional exact solid-solid Riemann solution structure can be presented as shown in Fig. 1.
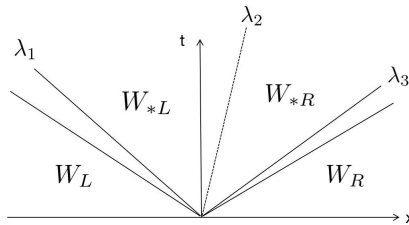


Figure 1: The exact three-wave solution structure of solid-solid Riemann solution.

Where, $W_L = (\rho_{*L}, u_{*L}, \sigma_{x*L})^T$ and $W_R = (\rho_{*R}, u_{*R}, \sigma_{x*R})^T$ are the unknown primitive constant variables on the left and right sides of the contact discontinuity.

As analysis in Section 2, $\lambda_1$-field and $\lambda_3$-field are genuinely non-linear, the corresponding wave can be either a rarefaction wave or a shock wave. If it is a rarefaction wave, according to (2.18) and (2.19), one can get

$$
\begin{aligned}
u_{*L} &= u_L - \sqrt{\frac{16\mu + 12K}{3\rho_L}} + \sqrt{\frac{16\mu + 12K}{3\rho_{*L}}}, \\
u_{*R} &= u_R + \sqrt{\frac{16\mu + 12K}{3\rho_R}} - \sqrt{\frac{16\mu + 12K}{3\rho_{*R}}},
\end{aligned}
\tag{3.1}
$$

where

$$
\rho_{*L} = \rho_L \exp\left(\frac{3\sigma_{xL} - 3\sigma_{x*L}}{4\mu + 3K}\right), \quad \rho_{*R} = \rho_R \exp\left(\frac{3\sigma_{xR} - 3\sigma_{x*R}}{4\mu + 3K}\right). \tag{3.2}
$$

Supposing $\lambda_1$-field and $\lambda_3$-field are both shock waves, the Rankine-Hugoniot condition across the elastic shock wave is

$$
\begin{aligned}
[\rho u] &= S[\rho], \\
[\rho u^2 - \sigma_x] &= S[\rho u],
\end{aligned}
\tag{3.3}
$$

where $S$ represents the shock wave speed. Applying (3.3) for the $\lambda_1$-field and $\lambda_3$-field respectively, we can obtain

$$
\begin{aligned}
u_{*L} &= u_L + \sqrt{(\sigma_{xL} - \sigma_{x*L})\left(\frac{1}{\rho_L} - \frac{1}{\rho_{*L}}\right)}, \\
u_{*R} &= u_R - \sqrt{(\sigma_{xR} - \sigma_{x*R})\left(\frac{1}{\rho_R} - \frac{1}{\rho_{*R}}\right)}.
\end{aligned}
\tag{3.4}
$$

For $\lambda_2$-field, due to (2.21), $\sigma_{x*L} = \sigma_{x*R}$ and $u_{*L} = u_{*R}$ hold. Then we can obtain the total stress $\sigma_{*L}$ and $\sigma_{*R}$ in the star region by solving a nonlinear algebraic equation, say, with the bisection method. The nonlinear algebraic equation is shown as follows:

$$
h(\sigma_{*L}.W_L, W_R) = g_L^e(\sigma_{*L}, W_L) + g_R^e(\sigma_{*R}, W_R) + u_R - u_L = 0, \tag{3.5}
$$

where the $g_L^e(\sigma_{*L}, W_L)$ and $g_R^e(\sigma_{*R}, W_R)$ are given by

$$
g_L^e(\sigma_{x*L}, W_L) = \begin{cases} \sqrt{(\sigma_L - \sigma_{x*L})\left(\dfrac{1}{\rho_L} - \dfrac{1}{\rho_{*L}}\right)}, & \text{if} \quad \sigma_{x*L} < \sigma_L, \\[2ex] \sqrt{\dfrac{16\mu + 12K}{3\rho_L}} - \sqrt{\dfrac{16\mu + 12K}{3\rho_{*L}}}, & \text{if} \quad \sigma_{x*L} \geq \sigma_L, \end{cases} \tag{3.6a}
$$

$$g_R^e\left(\sigma_{x*R}, W_R\right) = \begin{cases} \sqrt{\left(\sigma_R - \sigma_{x*R}\right)\left(\dfrac{1}{\rho_R} - \dfrac{1}{\rho_{*R}}\right)}, & \text{if} \quad \sigma_{x*R} < \sigma_R, \\[4mm] \sqrt{\dfrac{16\mu + 12K}{3\rho_R}} - \sqrt{\dfrac{16\mu + 12K}{3\rho_{*R}}}, & \text{if} \quad \sigma_{x*R} \geq \sigma_R, \end{cases} \tag{3.6b}$$

$$\rho_{*L} = \rho_L \exp\left(\frac{3\sigma_{xL} - 3\sigma_{x*L}}{4\mu + 3K}\right), \quad \rho_{*R} = \rho_R \exp\left(\frac{3\sigma_{xR} - 3\sigma_{x*R}}{4\mu + 3K}\right). \tag{3.6c}$$

Here, superscript $e$ denotes that the solid is elastic, subscripts "$L$" and "$R$" stand for the left and right constant states respectively. If the total stress $\sigma_{x*L}$ and $\sigma_{x*R}$ in the star region are known, thanks to (3.2) and (3.5), we can obtain

$$u_{*L} = u_{*R} = \frac{1}{2}\left(u_L + u_R\right) + \frac{1}{2}\left[g_R^e\left(\sigma_{*R}, W_R\right) - g_L^e\left(\sigma_{*L}, W_L\right)\right],$$

$$\rho_{*L} = \rho_L \exp\left(\frac{3\sigma_{xL} - 3\sigma_{x*L}}{4\mu + 3K}\right), \quad \rho_{*R} = \rho_R \exp\left(\frac{3\sigma_{xR} - 3\sigma_{x*R}}{4\mu + 3K}\right), \tag{3.7}$$

$$s_{x*L} = -\frac{4\mu}{3}\ln\frac{\rho_*}{\rho_L} + s_{xL}, \qquad s_{x*R} = -\frac{4\mu}{3}\ln\frac{\rho_*}{\rho_R} + s_{xR}.$$

## 4. HLL approximate Riemann solver for the augmented governing system

### 4.1. The HLL approximate Riemann solver

As shown in Fig. 2, the whole wave structure arising from the solution of Riemann problem is contained in the control volume $[x_L, x_R] \times [0, T]$, where $x_L$ and $x_R$ satisfy

$$x_L \leq S_L T, \quad x_R \geq S_R T. \tag{4.1}$$

Here, $S_L$ and $S_R$ are the slowest and fastest signal speeds perturbing the initial data states $U_L$ and $U_R$, respectively, and $T$ is the chosen time. The integral form of the conservation laws (2.10) in the control volume $[x_L, x_R] \times [0, T]$ reads

$$\int_{x_L}^{x_R} U(x, T)\mathrm{d}x = \int_{x_L}^{x_R} U(x, 0)\mathrm{d}x + \int_0^T \mathbf{F}\big(\mathbf{U}(x_L, t)\big)\mathrm{d}t - \int_0^T \mathbf{F}\big(\mathbf{U}(x_R, t)\big)\mathrm{d}t. \tag{4.2}$$
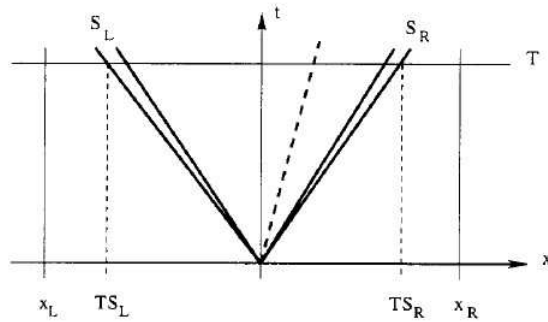


Figure 2: The HLL approximate Riemann solver.

The HLL approximate Riemann solver's conserved quantity in the star region [8] is defined by

$$\mathbf{U}^{hll} := \frac{1}{T(S_R - S_L)} \int_{TS_L}^{TS_R} \mathbf{U}(x,T)dx = \frac{S_R \mathbf{U}_R - S_L \mathbf{U}_L + F_L - F_R}{S_R - S_L}. \qquad (4.3)$$

Considering a control volume $[x_L, 0] \times [0, T]$, as shown in Fig. 2, integrating (2.10) in the above control volume, we can get

$$\int_{x_L}^{0} U(x,T)\mathrm{d}x = \int_{x_L}^{0} U(x,0)\mathrm{d}x + \int_{0}^{T} \mathbf{F}(\mathbf{U}(x_L,t))\,\mathrm{d}t - \int_{0}^{T} \mathbf{F}(\mathbf{U}(0,t))\,\mathrm{d}t. \qquad (4.4)$$

Combining (4.3) and (4.4), one can obtain

$$\mathbf{F}^{hll} := \mathbf{F}_R + S_R(\mathbf{U}^{hll} - \mathbf{U}_R) = \frac{S_R \mathbf{F}_L - S_L \mathbf{F}_R + S_L S_R (\mathbf{U}_R - \mathbf{U}_L)}{S_R - S_L}. \qquad (4.5)$$

The HLL approximate Riemann solver is then given as follows:

$$\widetilde{\mathbf{U}}(x,t) = \begin{cases} \mathbf{U}_L, & \text{if} \quad \dfrac{x}{t} \le S_L, \\ \mathbf{U}^{hll}, & \text{if} \quad S_L \le \dfrac{x}{t} \le S_R, \\ \mathbf{U}_R, & \text{if} \quad \dfrac{x}{t} \ge S_R, \end{cases} \quad \mathbf{U}^{hll} = \frac{S_R \mathbf{U}_R - S_L \mathbf{U}_L + F_L - F_R}{S_R - S_L}, \qquad (4.6)$$

$$\mathbf{F}^{hll} = \begin{cases} \mathbf{F}_L, & \text{if} \quad 0 \le S_L, \\ \dfrac{S_R \mathbf{F}_L - S_L \mathbf{F}_R + S_L S_R (\mathbf{U}_R - \mathbf{U}_L)}{S_R - S_L}, & \text{if} \quad S_L \le 0 \le S_R, \\ \mathbf{F}_R, & \text{if} \quad 0 \ge S_R. \end{cases} \qquad (4.7)$$

Where $\mathbf{F}_K = \mathbf{F}(U_K, s_K), K = L/R$. If the speeds of left- and right-going waves are given, we can evaluate all states in the star regions. Here we define the speeds of left- and right-going waves as

$$S_R = \max(u_L + c_L, u_R + c_R, 0), \quad S_L = \min(u_L - c_L, u_R - c_R, 0), \qquad (4.8)$$

where $c_L = \sqrt{\frac{4\mu + 3K}{3\rho_L}}$ and $c_R = \sqrt{\frac{4\mu + 3K}{3\rho_R}}$.

## 4.2. The discrepancy analysis for the HLL approximate Riemann solver

The numerical examples in the next section will show that non-physical oscillations occurring to the HLL approximate Riemann solver when directly applied to simulate the augmented linear elastic solid. We analyze the reason by defining a discrepancy factor that can be utilized to estimate the difference of the total stress across the contact discontinuity, where it is physically required to be continuous.

We assume that $W_L = (\rho_L, u_L, p_L, s_{xL})^T$, $W_R = (\rho_R, u_R, p_R, s_{xR})^T$ and $W^{hll} = (\rho^{hll}, u^{hll}, p^{hll}, s^{hll})^T$, where the variables in the star region are density $\rho^{hll}$, velocity $u^{hll}$, deviator stress $s^{hll}$ and pressure $p^{hll}$. They are known if the $\mathbf{U}^{\text{hll}}$ is given.

Thanks to (3.7) and (4.6), we can obtain

$$s_{x*L} := -\frac{4\mu}{3}\ln\frac{\rho^{hll}}{\rho_L} + s_{xL}, \quad s_{x*R} := -\frac{4\mu}{3}\ln\frac{\rho^{hll}}{\rho_R} + s_{xR}, \tag{4.9}$$

$$p_{x*L} := K\ln\frac{\rho^{hll}}{\rho_L} + p_{xL}, \qquad p_{x*R} := K\ln\frac{\rho^{hll}}{\rho_R} + p_{xR}. \tag{4.10}$$

Using (2.12), we can get

$$\sigma_{x*L} = -p_{x*L} + s_{x*L}, \quad \sigma_{x*R} = -p_{x*R} + s_{x*R}. \tag{4.11}$$

Substituting (4.9) and (4.10) into (4.11) yields

$$\sigma_{x*L} = \sigma_{xL} - \left(\frac{4\mu}{3} + K\right)\ln\frac{\rho^{hll}}{\rho_L}, \tag{4.12}$$

$$\sigma_{x*R} = \sigma_{xR} - \left(\frac{4\mu}{3} + K\right)\ln\frac{\rho^{hll}}{\rho_R}, \tag{4.13}$$

where

$$\rho^{hll} = \frac{S_R\rho_R - S_L\rho_L + \rho_L u_L - \rho_R u_R}{S_R - S_L}. \tag{4.14}$$

Then we define a discrepancy factor $\eta$, which is

$$\theta_1 = \left|\frac{\sigma_{x*L} - \sigma_{x*R}}{\sigma_{x*L}}\right|, \quad \theta_2 = \left|\frac{\sigma_{x*L} - \sigma_{x*R}}{\sigma_{x*R}}\right|, \tag{4.15}$$

$$\eta := \max\{\theta_1, \theta_2\}. \tag{4.16}$$

To describe the discrepancy degree of the HLL approximate Riemann solver, we expand the formula (4.16) in detail. Substituting (4.12)-(4.15) into (4.16) yields

$$\eta := \max\left\{\left|\frac{\sigma_{xL} - \sigma_{xR}}{\sigma_{xL} - \left(\frac{4\mu}{3} + K\right)\ln\left(1 + \frac{u_L - u_R}{S_R - S_L}\right)}\right|, \right.$$
$$\left.\left|\frac{\sigma_{xL} - \sigma_{xR}}{\sigma_{xR} - \left(\frac{4\mu}{3} + K\right)\ln\left(1 + \frac{u_L - u_R}{S_R - S_L}\right)}\right|\right\}, \tag{4.17}$$

if $\rho_L = \rho_R$. Based on (4.17), we discuss the influence of different initial conditions on the HLL approximate Riemann solver by using the discrepancy factor. In general, the speed of sound $c_L$ and $c_R$ are much larger than the initial velocity $u_L$ and $u_R$. In the premise of ignoring high-speed collision which usually leads to plastic deformation, we can obtain

$$\ln\left(1 + \frac{u_L - u_R}{S_R - S_L}\right) \to 0 \tag{4.18}$$

with

$$c_R + c_L \gg |u_R - u_L|.$$

Thus if $c_R + c_L \gg |u_R - u_L|$ holds, the discrepancy factor $\eta$ is mainly determined by $(\sigma_{xL} - \sigma_{xR})/\sigma_{xL}$ and $(\sigma_{xL} - \sigma_{xR})/\sigma_{xR}$. Because the $4\mu/3 + K$ is a large number for solid, as $|u_R - u_L|$ grows larger, its effect on the discrepancy factor cannot be ignored. Based on the above discussion, the discrepancy factor can be refined as follows:

$$\eta = \begin{cases} \max\left\{ \left| \dfrac{\sigma_{xL} - \sigma_{xR}}{\sigma_{xL}} \right|, \left| \dfrac{\sigma_{xL} - \sigma_{xR}}{\sigma_{xR}} \right| \right\}, & \text{if} \quad c_R + c_L \gg |u_R - u_L|, \\[2em] \max\left\{ \left| \dfrac{\sigma_{xL} - \sigma_{xR}}{\sigma_{xL} - \left(\frac{4\mu}{3} + K\right) \ln\left(1 + \frac{u_L - u_R}{S_R - S_L}\right)} \right|, \right. \\ \left. \left| \dfrac{\sigma_{xL} - \sigma_{xR}}{\sigma_{xR} - \left(\frac{4\mu}{3} + K\right) \ln\left(1 + \frac{u_L - u_R}{S_R - S_L}\right)} \right| \right\}, & \text{others.} \end{cases} \tag{4.19}$$

According to (4.19), if $\sigma_{xL} = \sigma_{xR}$ holds, we can get $\eta = 0$. If not, the discrepancy of the total stress across the contact discontinuity appears, which is against the physical requirement. The larger the initial difference of the total stress is, the higher the discrepancy factor is.

## 5. HLLC approximate Riemann solver for the augmented governing system

### 5.1. The HLLC approximate Riemann solver

As shown in Fig. 3, the whole wave structure arising from the solution of the Riemann problem is contained in the control volume $[x_L, x_R] \times [0, T]$. Now, in addition to the slowest and fastest signal speeds $S_L$ and $S_R$, we include a middle wave of the speed $S_*$.

Evaluation of the integral form of the conservation laws in the control volume reproduces the result of Eq. (4.3), even if variations of the integrand across the wave of the speed $S_*$ are allowed. By splitting the left-hand side of integral (4.3) into two
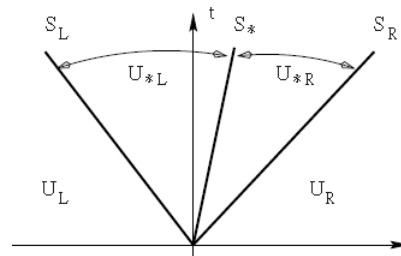


Figure 3: The HLLC approximate Riemann solver.

terms, we can obtain

$$\frac{1}{T(S_R - S_L)} \int_{TS_L}^{TS_R} \mathbf{U}(x, T) dx$$

$$= \frac{1}{T(S_R - S_L)} \int_{TS_L}^{TS_*} \mathbf{U}(x, T) \mathrm{d}x + \frac{1}{T(S_R - S_L)} \int_{TS_*}^{TS_R} \mathbf{U}(x, T) \mathrm{d}x. \quad (5.1)$$

Defining the integral averages

$$U_{*L} = \frac{1}{T(S_R - S_L)} \int_{TS_L}^{TS_*} \mathbf{U}(x, T) \mathrm{d}x,$$

$$U_{*R} = \frac{1}{T(S_R - S_L)} \int_{TS_*}^{TS_R} \mathbf{U}(x, T) \mathrm{d}x \quad (5.2)$$

with (4.3), (5.1) and (5.2), one can have

$$\frac{S_* - S_L}{S_R - S_L} U_{*L} + \frac{S_R - S_*}{S_R - S_L} U_{*R} = U^{\mathrm{HLL}}. \quad (5.3)$$

Applying Rankine-Hugoniot conditions across each wave with respective speeds $S_L$, $S_R$ and $S_*$, we can get

$$\mathbf{F}_{*L} = \mathbf{F}_L + S_L (U_{*L} - U_L), \quad (5.4)$$

$$\mathbf{F}_{*R} = \mathbf{F}_{*L} + S_* (U_{*R} - U_{*L}), \quad (5.5)$$

$$\mathbf{F}_{*R} = \mathbf{F}_R + S_R (U_{*R} - U_R). \quad (5.6)$$

The middle wave with speed $S_*$ is assumed to be a contact discontinuity, for pressure and velocity we have

$$p_{*L} = p_{*R} = p_*, \quad u_{*L} = u_{*R} = u_*. \quad (5.7)$$

In addition, it is entirely convenient to set

$$S_* = u_*. \quad (5.8)$$

By using (5.3)-(5.8), the HLLC approximate Riemann solver is given as follows:

$$\widetilde{\mathbf{U}}(x, t) = \begin{cases} \mathbf{U}_L, & \text{if} \quad \dfrac{x}{t} \leq S_L, \\ \mathbf{U}_{*L}, & \text{if} \quad S_L \leq \dfrac{x}{t} \leq S_*, \\ \mathbf{U}_{*R}, & \text{if} \quad S_* \leq \dfrac{x}{t} \leq S_R, \\ \mathbf{U}_R, & \text{if} \quad \dfrac{x}{t} \geq S_R, \end{cases} \quad (5.9)$$

where

$$U_{*L} = \frac{S_L U_L - F_L + p_{*L} D_*}{S_L - S_*},$$

$$U_{*R} = \frac{S_R U_R - F_R + p_{*R} D_*}{S_L - S_*}, \quad (5.10)$$

and $D_* = [0, 1, S_*]^T$. A corresponding HLLC numerical flux [8] in the Eulerian framework is defined as

$$\mathbf{F}^{HLLC} = \begin{cases} \mathbf{F}_L, & \text{if} \quad 0 \leq S_L, \\ \mathbf{F}_{*L}, & \text{if} \quad S_L \leq 0 \leq S_*, \\ \mathbf{F}_{*R}, & \text{if} \quad S_* \leq 0 \leq S_R, \\ \mathbf{F}_R, & \text{if} \quad 0 \geq S_R, \end{cases} \tag{5.11}$$

where

$$\mathbf{F}_{*K} = \mathbf{F}(U_{*K}, s_{*K}), \quad \mathbf{F}_K = \mathbf{F}(U_K, s_K), \quad K = L, R, \tag{5.12}$$

$$S_* = \frac{p_R - p_L + \rho_L u_L (S_L - u_L) - \rho_R u_R (S_R - u_R)}{\rho_L (S_L - u_L) - \rho_R (S_R - u_R)}. \tag{5.13}$$

The deviator stress in the star region is computed by

$$s_{x*L} = -\frac{4\mu}{3} \ln \frac{\rho_{*L}}{\rho_L} + s_{xL}, \quad s_{x*R} = -\frac{4\mu}{3} \ln \frac{\rho_{*L}}{\rho_R} + s_{xR}. \tag{5.14}$$

## 5.2. The discrepancy analysis for the HLLC approximate Riemann solver

The numerical examples in the next section will show that the non-physical oscillations occurring to the HLLC approximate Riemann solver when directly applied to simulate the augmented linear elastic solid. Here, we analyze the insightful reason by using the discrepancy factor defined above.

We assume that $W_L = (\rho_L, u_L, p_L, s_{xL})^T$, $W_R = (\rho_R, u_R, p_R, s_{xR})^T$ and $W_{*L} = (\rho_{*L}, u_{*L}, p_{*L}, s_{x*L})^T$, $W_{*R} = (\rho_{*R}, u_{*R}, p_{*R}, s_{x*R})^T$, where the meanings of above subscripts "$L$", "$*L$", "$*R$", "$R$", "$xL$", "$x*L$", "$x*R$", "$xR$" are the same as shown in Fig. 1.

There are two ways to construct HLLC approximate Riemannian solver in detail. The first is to use the fluid approximate Riemann solver directly, ignoring the effect of deviatoric stress. According to reference [8], we get that

$$p_{*L} = p_L + \rho_L (S_L - u_L)(S_* - u_L), \quad p_{*R} = p_R + \rho_R (S_R - u_R)(S_* - u_R). \tag{5.15}$$

At the left and right sides of the contact discontinuity, applying (2.12), we can have

$$\sigma_{x*L} = -p_{*L} + s_{x*L}, \quad \sigma_{x*R} = -p_{*R} + s_{x*R}. \tag{5.16}$$

Substituting (5.14), (5.15) into (5.16) yields,

$$\sigma_{x*L} = \sigma_{xL} - \frac{4\mu}{3} \ln \frac{\rho_{*L}}{\rho_L} - \rho_L (S_L - u_L)(S_* - u_L), \tag{5.17}$$

$$\sigma_{x*R} = \sigma_{xR} - \frac{4\mu}{3} \ln \frac{\rho_{*R}}{\rho_R} - \rho_R (S_R - u_R)(S_* - u_R). \tag{5.18}$$

Subtracting (5.17) from (5.18), we can obtain

$$\sigma_{x*L} - \sigma_{x*R} = \sigma_{xL} - \sigma_{xR} + \frac{4\mu}{3}\left(\ln\frac{\rho_{*R}}{\rho_R} - \ln\frac{\rho_{*L}}{\rho_L}\right) + \rho_R\left(S_R - u_R\right)\left(S_* - u_R\right)$$
$$- \rho_L\left(S_L - u_L\right)\left(S_* - u_L\right), \tag{5.19}$$

where

$$\rho_{*L} = \rho_L\left(\frac{S_L - u_L}{S_L - S_*}\right), \quad \rho_{*R} = \rho_R\left(\frac{S_R - u_R}{S_R - S_*}\right). \tag{5.20}$$

Then we can compute the discrepancy factor $\eta$ as defined in the (4.16) in detail. Supposing $\rho_L = \rho_R$, substituting (5.17)-(5.20) into (4.16) yields

$$\eta := \max\left\{\left|\frac{\sigma_{xL}-\sigma_{xR}+\frac{4\mu}{3}\ln\frac{(S_R-u_R)(S_L-S_*)}{(S_R-S_*)(S_L-u_L)}+\rho_R(S_R-u_R)(S_*-u_R)-\rho_L(S_L-u_L)(S_*-u_L)}{\sigma_{xR}-\frac{4\mu}{3}\ln\left(\frac{S_R-u_R}{S_R-S_*}\right)-\rho_R(S_R-u_R)(S_*-u_R)}\right|, \atop \left|\frac{\sigma_{xL}-\sigma_{xR}+\frac{4\mu}{3}\ln\frac{(S_R-u_R)(S_L-S_*)}{(S_R-S_*)(S_L-u_L)}+\rho_R(S_R-u_R)(S_*-u_R)-\rho_L(S_L-u_L)(S_*-u_L)}{\sigma_{xL}-\frac{4\mu}{3}\ln\left(\frac{S_L-u_L}{S_L-S_*}\right)-\rho_L(S_L-u_L)(S_*-u_L)}\right|\right\}. \tag{5.21}$$

The second is to adopt the method of reference [3]. From (5.4)-(5.6), one can obtain

$$p_{*L} = p_L + \rho_L\left(S_L - u_L\right)\left(s^* + s_{x*L} - u_L\right),$$
$$p_{*R} = p_R + \rho_R\left(S_R - u_R\right)\left(s^* + s_{x*R} - u_R\right), \tag{5.22}$$

where

$$s^* = \frac{p_R - p_L + \rho_L\left(u_L - s_{x*L}\right)\left(S_L - u_L\right) - \rho_R\left(u_R - s_{x*R}\right)\left(S_R - u_R\right)}{\rho_L\left(S_L - u_L\right) - \rho_R\left(S_R - u_R\right)}, \tag{5.23}$$

$$s_{x*L} = \frac{s^*_{xx,\,L} - s_{xL}}{\rho_L\left(s_L - u_L\right)}, \qquad s_{x*R} = \frac{s^*_{xx,R} - s_{xR}}{\rho_R\left(s_R - u_R\right)}, \tag{5.24}$$

$$s^*_{xx,\,L} = s_{x\,L} + \rho_L\left(s_L - u_L\right)\widetilde{s}^*_x, \quad s^*_{xx,R} = s_{xR} + \rho_R\left(s_R - u_R\right)\widetilde{s}^*_x,$$

$$\widetilde{s}^*_x = \frac{s_{xR} - s_{xL}}{\rho_L\left(s_L - u_L\right) - \rho_R\left(s_R - u_R\right)}.$$

Combining (5.16) and (5.22)-(5.24), we can get

$$\sigma_{*L} = -p_L - \rho_L\left(S_L - u_L\right)\left(s^* + s_{x*L} - u_L\right) + \frac{s^*_{xx,\,L} - s_{xL}}{\rho_L\left(s_L - u_L\right)},$$

$$\sigma_{*R} = -p_R - \rho_R\left(S_R - u_R\right)\left(s^* - s_{x*R} - u_R\right) + \frac{s^*_{xx,R} - s_{xR}}{\rho_R\left(s_R - u_R\right)}, \tag{5.25}$$

$$\sigma_{x*L} - \sigma_{x*R} = \left(p_R - p_L\right) + \rho_R\left(S_R - u_R\right)\left(s^* - s_{x*R} - u_R\right) - \rho_L,$$

$$\left(S_L - u_L\right)\left(s^* + s_{x*L} - u_L\right) + \frac{s^*_{xx,R} - s_{xR}}{\rho_R\left(s_R - u_R\right)} - \frac{s^*_{xx,\,L} - s_{xL}}{\rho_L\left(s_L - u_L\right)}. \tag{5.26}$$

Supposing $\rho_L = \rho_R$ and substituting (5.25)-(5.26) into (4.16) yields

$$\eta := \max\left(\left|\frac{\sigma_{x*L} - \sigma_{x*R}}{\sigma_{x*L}}\right|, \left|\frac{\sigma_{x*L} - \sigma_{x*R}}{\sigma_{x*R}}\right|\right). \tag{5.27}$$

According to (5.21) and (5.27), if the $\eta \neq 0$ holds, it means that the total stress is not continuous across a contact discontinuity, which goes against the physical requirement. One may have realized that the appearance of discrepancy is due to the wrong imposition of pressure continuity across the contact discontinuity in the previous literature. Such a defect has been fixed in the MHLLCEP [17] by enforcing the continuity of total stress across the contact discontinuity. In the next section, we will propose a linearized double-shock approximate Riemann solver, which can naturally hold continuity of total stress there.

## 6. Linearized double-shock approximate Riemann solver for the augmented governing system

To overcome the shortcomings of the popular HLL and HLLC approximate Riemann solvers, we present a linearized double-shock approximation solver. The structure of the solution is the same as shown in Fig. 1, in which the nonlinear waves are assumed both shock waves.

In (3.6) Taylor expansion yields

$$\sqrt{(\sigma_{xL} - \sigma_{x*L})\left(\frac{1}{\rho_L} - \frac{1}{\rho_{*L}}\right)} = -\frac{\sigma_{xL}}{c_L\rho_L}\left(\frac{\sigma_{x*L}}{\sigma_{xL}} - 1\right) + \mathcal{O}\left(\frac{\sigma_{x*L}}{\sigma_{xL}} - 1\right)^2, \tag{6.1}$$

$$\sqrt{(\sigma_{xR} - \sigma_{x*R})\left(\frac{1}{\rho_R} - \frac{1}{\rho_{*R}}\right)} = -\frac{\sigma_{xR}}{c_R\rho_R}\left(\frac{\sigma_{x*R}}{\sigma_{xR}} - 1\right) + \mathcal{O}\left(\frac{\sigma_{x*R}}{\sigma_{xR}} - 1\right)^2. \tag{6.2}$$

Taking the leading term of (6.1) and (6.2), we have

$$\sqrt{(\sigma_{xL} - \sigma_{x*L})\left(\frac{1}{\rho_L} - \frac{1}{\rho_{x*L}}\right)} = -\frac{\sigma_{xL}}{c_L\rho_L}\left(\frac{\sigma_{x*L}}{\sigma_{xL}} - 1\right), \tag{6.3}$$

$$\sqrt{(\sigma_{xR} - \sigma_{x*R})\left(\frac{1}{\rho_R} - \frac{1}{\rho_{*R}}\right)} = -\frac{\sigma_{xR}}{c_R\rho_R}\left(\frac{\sigma_{x*R}}{\sigma_{xR}} - 1\right). \tag{6.4}$$

Substituting (6.3) and (6.4) into (3.5), one can get

$$\sigma_{x*L} = \sigma_{x*R} = \frac{1}{\frac{1}{c_R\rho_R} + \frac{1}{c_L\rho_L}}\left(\frac{\sigma_{xR}}{c_R\rho_R} + \frac{\sigma_{xL}}{c_L\rho_L}\right) + u_R - u_L. \tag{6.5}$$

Substituting (6.3)-(6.5) into (3.7), we can obtain

$$u_{*L} = u_{*R} = \frac{1}{2}(u_L + u_R) + \frac{1}{2}\left[\frac{\sigma_{xL}}{c_L\rho_L}\left(\frac{\sigma_{x*L}}{\sigma_{xL}} - 1\right) - \frac{\sigma_R}{c_R\rho_R}\left(\frac{\sigma_{x*R}}{\sigma_{xR}} - 1\right)\right], \tag{6.6}$$

$$\rho_{*L} = \rho_L \exp\left(\frac{3\sigma_{xL} - 3\sigma_{x*L}}{4\mu + 3K}\right), \quad \rho_{*R} = \rho_R \exp\left(\frac{3\sigma_{xR} - 3\sigma_{x*R}}{4\mu + 3K}\right), \tag{6.7}$$

$$s_{x*L} = -\frac{4\mu}{3}\ln\frac{\rho_{*L}}{\rho_L} + s_{xL}, \qquad s_{x*R} = -\frac{4\mu}{3}\ln\frac{\rho_{*R}}{\rho_R} + s_{xR}. \tag{6.8}$$

According to reference [9], when $|\sigma_I/\sigma_K - 1| < 1$, for the elastic wave connecting $W_K$ with $W_{*K}$, $\sigma_{x*K}$ calculated by (6.5) approximates its exact solution $\sigma_{x*K}^e$ to the accuracy of $\mathcal{O}(\sigma_I/\sigma_{xL} - 1)^2 + \mathcal{O}(\sigma_I/\sigma_{xR} - 1)^2$, $u_{*K}$ calculated by (6.6) approximates its exact solution $u_{*K}^e$ to the accuracy of $\mathcal{O}(\sigma_I/\sigma_{xL} - 1)^2 - \mathcal{O}(\sigma_I/\sigma_{xR} - 1)^2$.

We calculate the discrepancy factor $\eta$ for the linearized double-shock approximate Riemann solver. Substituting (6.5) into (4.16), one can obtain

$$\theta_1 = 0, \quad \theta_2 = 0, \quad \eta = 0. \tag{6.9}$$

Thus no matter what the initial conditions are, the $\eta = 0$ always holds for the linearized double-shock approximate Riemann solver, which means that the total stress is always continuous across a contact discontinuity under the linearized double-shock approximate Riemann solver.

## 7. Numerical performance testing of approximate Riemann solvers

In this section, the HLLC approximate Riemann solver in reference [3] is proposed for elastic-plastic flows in solid for comparison. We test the HLL, HLLC, and linearized double-shock approximate Riemann solvers to demonstrate that the discrepancy factor can be used as an index to measure the magnitude of the non-physical oscillations. If $\eta = 0$ holds, There are no non-physical oscillations in the numerical simulation. If not, the non-physical oscillations will become more obvious when $\eta$ increases.

In order to obtain numerical results, we use the following numerical algorithm.

---
**Algorithm 7.1**

---
    **Step 1.**    Inputting the initial constant states $U_L, U_R$ and material parameters for the solid.

    **Step 2.**    Obtaining the flux $F_{i\pm\frac{1}{2}}$ by using approximation Riemann solver.

    **Step 3.**    Obtaining the $U^{n+1}$ by using $U_{ij}^{n+1} = U_{ij}^n - \frac{\Delta t}{\Delta x}(F_{i+\frac{1}{2}} - F_{i-\frac{1}{2}})$.

    **Step 4.**    The stress can be obtained by the formula $s_{x,i}^{n+1} = s_{x,i}^n - \Delta t \frac{4\mu}{3} \ln \frac{\rho^{n+1}}{\rho^n}$.

---

In the following numerical tests, the solid material is aluminum with physical constant parameters $\gamma = 2.67$, $c_0 = 5380.0\,m/s$, $\rho_0 = 2710.0\,kg/m^3$, K $= 7400.0\,Mpa$, $\mu = 2650.0\,Mpa$, $Y_0 = 300.0\,Mpa$. After the nondimensionalization, these parameters are transformed into $\gamma = 2.67$, $c_0 = 538.0$, $\rho_0 = 2.71$, K $= 740000.0$, $\mu = 265000$, $Y_0 = 3000.0$. The numerical results can be compared with the exact solution [10]. The computational domain is set to be $[0.0, 4.0]$ with 3000 uniform grid points and the initial interface is located at $2.0$. Besides, the CFL number is $0.2$ and the terminal time is $0.001$. Below, in the figures, the legends of HLL, HLLC and Double-Shock represent the numerical results simulated with HLL, HLLC and the linearized double-shock approximate Riemann solvers, respectively.

**Test 1. Numerical test of $\eta = 0.0$.** Its Riemann problem solution type is "$S_E|S_E$". The nondimensional initial conditions are

$$\begin{aligned}
u_L &= 2.0, & p_L &= 1.0, & s_L &= 0.0, & \rho_L &= 2.7, \\
u_R &= -1.0, & p_R &= 1.0, & s_R &= 0.0, & \rho_R &= 2.7.
\end{aligned} \tag{7.1}$$

For the case of test 1, the $\sigma_{xL} - \sigma_{xR} = 0$ holds, which means that discrepancy factor $\eta$ equals zero for the HLL and HLLC schemes. As shown in Fig. 4, there are no non-physical oscillations in the region of interface for all three approximate Riemann solvers.
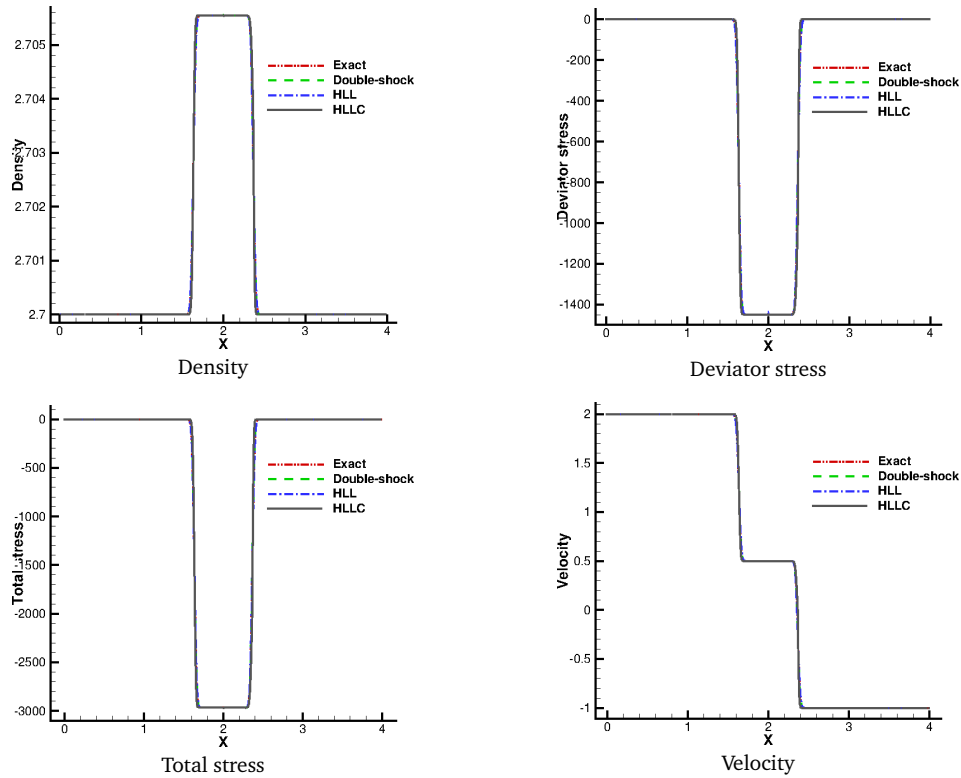


Figure 4: Numerical test of $\eta = 0.0$ (test 1).

**Test 2. Numerical test of $\eta \neq 0.0$.** The nondimensional initial conditions are

$$\begin{aligned}
u_L &= 2.0, & p_L &= 1.0, & s_L &= -500.0, & \rho_L &= 2.7, \\
u_R &= -1.0, & p_R &= 1.0, & s_R &= 0.0, & \rho_R &= 2.7.
\end{aligned} \tag{7.2}$$

For test 2, the initial difference of total stress is not zero. As a result, the discrepancy factors are not zero for both the HLL and HLLC solvers. As shown in Fig. 5, we can see that non-physical oscillations occurring to the HLL and HLLC solvers in the region of the interface. The non-physical oscillations inevitably appear in the vicinity of contact discontinuity if this factor is away from zero for the HLL and HLLC approximate
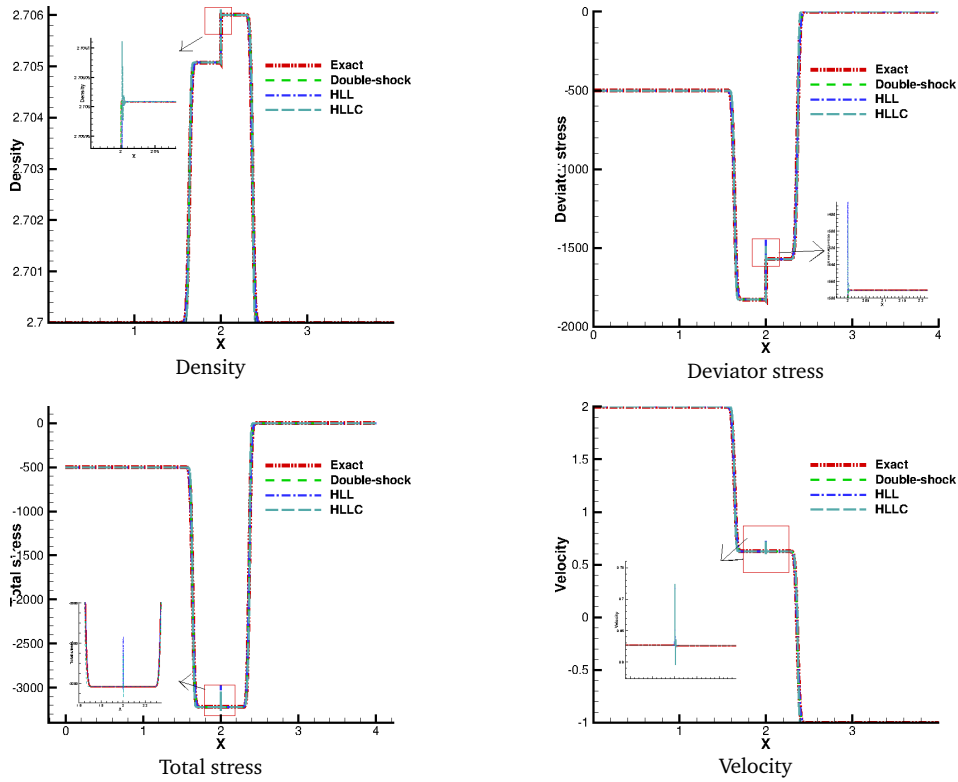
Figure 5: Numerical test of $\eta \neq 0.0$ (test 2).

Riemann solvers, and the linearized double-shock approximate Riemann solver can eliminate these non-physical oscillations effectively.

**Test 3. Numerical test of $\eta \neq 0.0$.** The nondimensional initial conditions are

$$
\begin{aligned}
u_L &= 2.0, & p_L &= 1.0, & s_L &= -1400.0, & \rho_L &= 2.7, \\
u_R &= -1.0, & p_R &= 1.0, & s_R &= 0.0, & \rho_R &= 2.7.
\end{aligned}
\tag{7.3}
$$

For test 3, we increase the difference of initial total stress to $\sigma_{xL} - \sigma_{xR} = -1400$. As shown in Fig. 6, severe non-physical oscillations occur in the vicinity of the interface for the HLL and HLLC approximate Riemann problem solvers, as the discrepancy factor $\eta$ goes larger. There are still no non-physical oscillations happening to the linearized double-shock approximate Riemann solver.

**Test 4. Two-dimensional linear elastic solid interaction.** A semi-infinite long aluminum target with a non-dimensional velocity of $2$ impacts on a semi-infinite aluminum target in two dimensions. The entire non-dimensional computational domain is a square region $x \times y \in [0,4] \times [0,2]$, comprising a rectangle region $x \times y \in [0,2] \times [0,2]$ for the left semi-infinite long aluminum target and a rectangle region $x \times y \in [2,4] \times [0,2]$ for the right semi-infinite aluminum target at the time $t = 0$. A total of $300 \times 200$

Density



Deviator stress



Total stress



Velocity
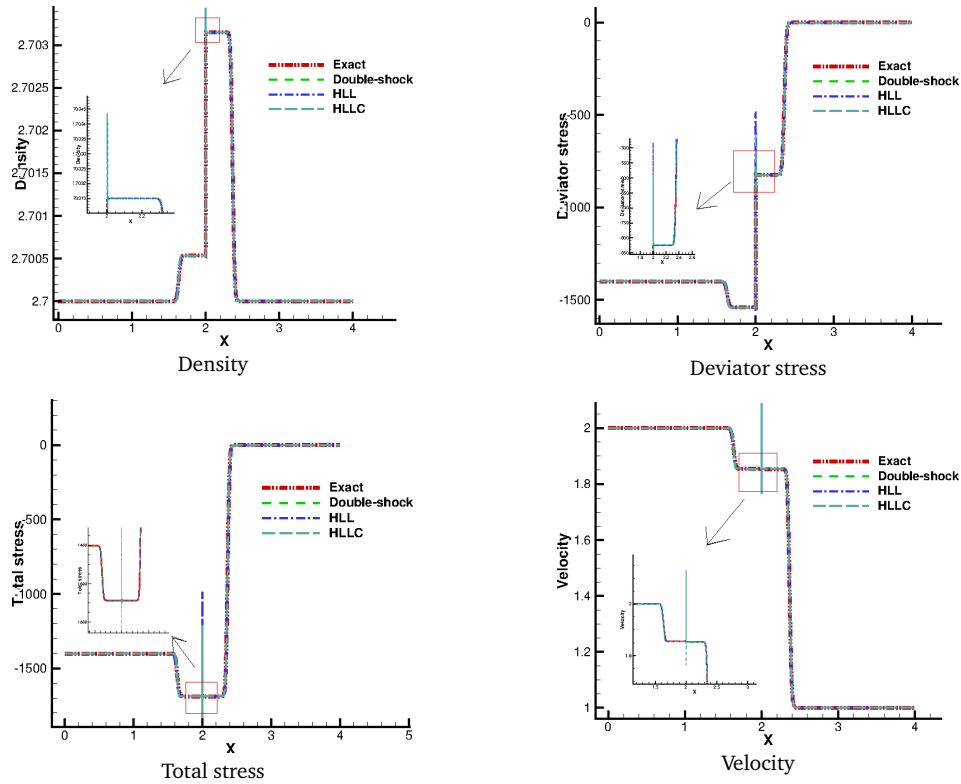
Figure 6: Numerical test of $\eta \neq 0.0$ (test 3).



Y-direction deviator stress



X-direction velocity
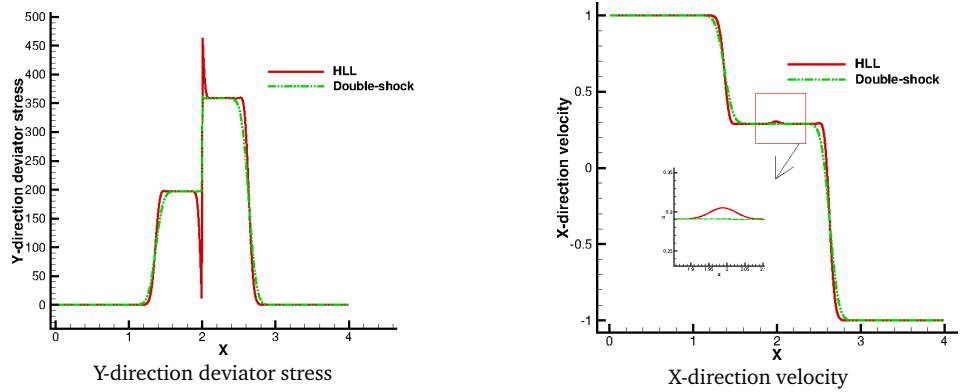
Figure 7: Numerical result comparison of different approximate Riemann solvers (test 4).

uniform grid points are distributed in the whole computational domain. The CFL is set to be $0.4$ and the terminal time is $0.001$. The non-dimensional initial conditions for the semi-infinite long aluminum target are

$$
\begin{aligned}
&u_L = 1.0, \quad\ \ v_L = 0.0, \ \ p_L = 1.0, \ \ s_{xL} = -1000.0, \ s_{yL} = s_{xyL} = 0.0, \ \rho_L = 2.7, \\
&u_R = -1.0, \quad v_R = 0.0, \ p_R = 1.0, \ \ s_{xR} = s_{yR} = s_{xyR} = 0.0, \ \rho_R = 2.7.
\end{aligned}
\tag{7.4}
$$

Density



X-direction deviator stress



Y-direction deviator stress



X-direction velocity



Y-direction velocity



Shear



Pressure
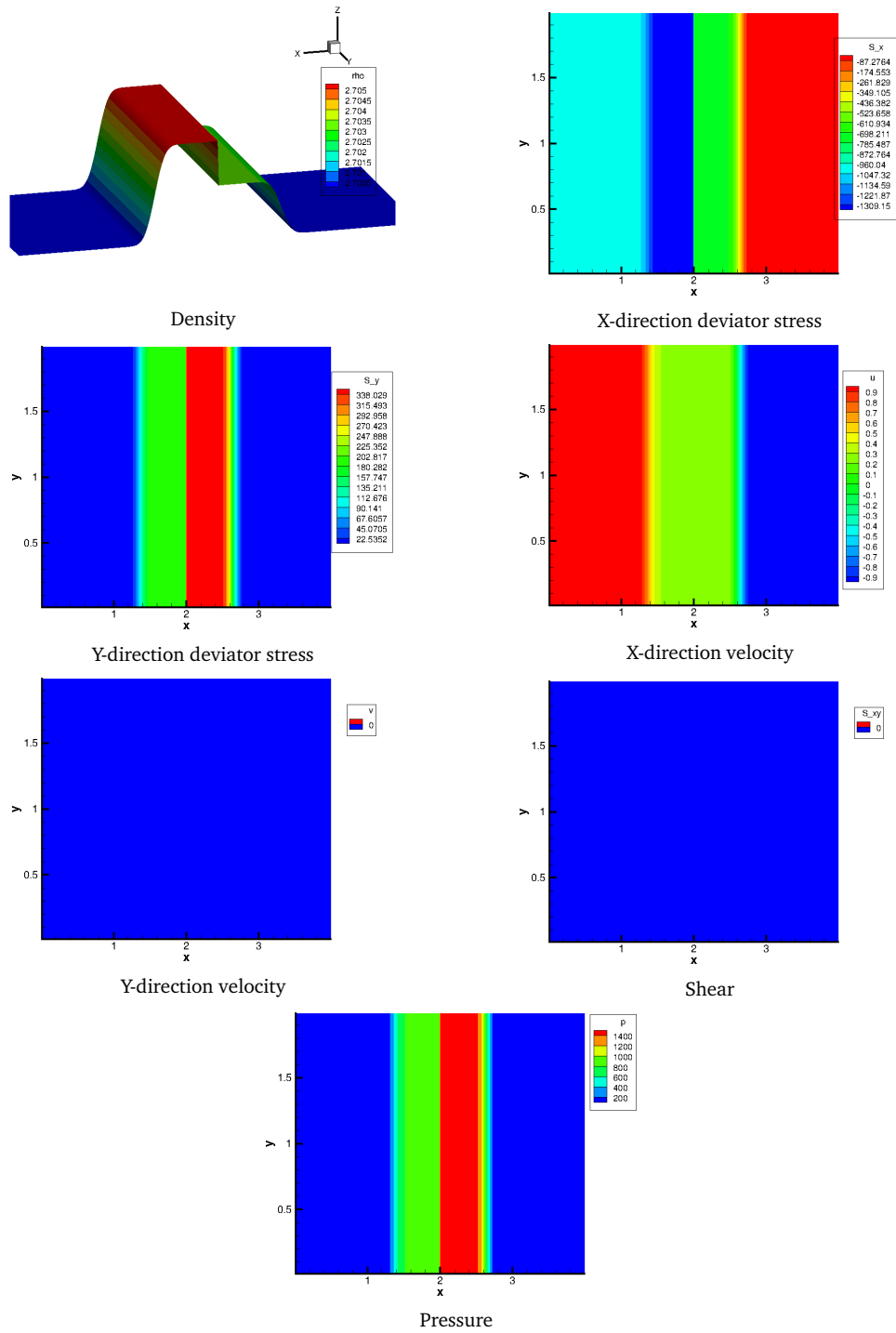
Figure 8: Numerical simulation of a 2 m/s semi-infinite long aluminum target impacting on a semi-infinite aluminum target in two dimensions (test 4).

For this two-dimensional numerical test, in order to compare the numerical results of the HLL and linearized double-shock approximate Riemann solvers clearly, the $x$-direction velocity and $y$-direction deviator stress are displayed in Fig. 7. We can discover that there are acute non-physical oscillations near the interface for the HLL approximate Riemann solver. As always, the linearized double-shock approximate Riemann solver eliminates non-physical oscillations in the numerical simulation.

The contours of other physical quantities are shown in Fig. 8 for the present method. Numerical results demonstrate that the linearized double-shock approximate Riemann solver can be extended to a two-dimensional augmented linear elastic solid.

## 8. Conclusions

In this work, augmented energy was constructed by utilizing Hooke's law and the first law of thermodynamics for the one-dimensional linear elastic solid. The non-conservative elastic system can be rewritten into a conservation form with the help of augmented energy. We analyzed the insightful reason why non-physical oscillations occur to the popular HLL and HLLC approximate Riemann solvers by defining a discrepancy factor $\eta$. A linearized double-shock approximate Riemann solver was proposed to heal such difficulty successfully. We believe that the discrepancy factor $\eta$ can also be extended to analyze the elastic-plastic Riemann solver in future work and the linearized double-shock approximate Riemann solver can be applied to simulate the elastic-plastic flows in solid.

## Acknowledgments

## References

[1] P. T. BARTON, D. DRIKAKIS, E. ROMENSKI, V. A. TITAREV, *Exact and approximate solutions of Riemann problems in non-linear elasticity*, J. Comput. Phys. 228(18) (2009), 7046–7068.

[2] L. CHEN, R. LI, C. YAO, *An approximate Riemann solver for fluid-solid interaction problems with Mie-Grüneisen equations of state*, Commun. Comput. Phys. 27(3) (2020), 861–896.

[3] J. CHENG, *Harten-Lax-van Leer-contact (HLLC) approximation Riemann solver with elastic waves for one-dimensional elastic-plastic problems*, Appl. Math. Mech. (English Ed.) 37(11) (2016), 117–138.

[4] J. B. CHENG, E. F. TORO, S. JIANG, M. YU, AND W. TANG, *A high-order cell-centered lagrangian scheme for one-dimensional elastic–plastic problems*, Comput. & Fluids 122 (2015), 136–152.

[5] J. K. DUKOWICZ, *A general non-iterative Riemann solver for Godunov method*, J. Comput. Phys. 61(1) (1985), 119–137.

[6] B. EINFELDT, *On Godunov-type methods for gas dynamics*, SIAM J. Numer. Anal. 25(2) (1988), 294–318.

[7] B. EINFELDT, C. D. MUNZ, P. L. ROE, B. SJÖGREEN, *On Godunov-type methods near low densities*, J. Comput. Phys. 92(2) (1991), 273–295.

[8] F. T. ELEUTERIO, *Riemann Solvers and Numerical Methods for Fluid Dynamics*, Springer, (1997).

[9] S. GAO, T. LIU, *A solution structure-based adaptive approximate (SSAA) Riemann solver for the elastic-perfectly plastic solid*, Commun. Comput. Phys. 25(3) (2019), 781–811.

[10] S. GAO, T. LIU, C. YAO, *A complete list of exact solutions for one-dimensional elastic-perfectly plastic solid Riemann problem without vacuum*, Commun. Nonlinear Sci. Numer. Simul. 63 (2018), 205–227.

[11] X. GARAIZAR, *Solution of a Riemann problem for elasticity*, J. Elasticity 26(1) (1991), 43–63.

[12] S. L. GAVRILYUK, N. FAVRIE, AND R. SAUREL, *Modeling wave dynamics of compressible elastic materials*, J. Comput. Phys. 227 (2008), 2941-–2969.

[13] S. K. GODUNOV, *A finite difference method for the computation of discontinuous solutions of the equations of fluid dynamics*, Sbornik: Mathematics 47 (1959), 357-–93.

[14] A. HARTEN, P. D. LAX, B. V. LEER, *On upstream differencing and Godunov-type schemes for hyperbolic conservation laws*, SIAM Rev. 25(1) (1983), 35–61.

[15] P. G. LEFLOCH, F. OLSSON, *A second-order Godunov method for the conservation laws of nonlinear elastidynamics*, IMPACT of Computing in Science and Engineering 2 (1990), 318–354.

[16] X. LI, C. SIN, Z. SHEN, *Numerical simulation of one-dimensional elastic-perfectly plastic flow and suppression of wall heating phenomenon,* Chinese J. Comput. Phys. 37(5) (2020), 539–50.

[17] L. LIU, J. B. CHENG, Z. LIU, *A multi-material HLLC Riemann solver with both elastic and plastic waves for 1D elastic-plastic flows*, Comput. & Fluids 192 (2019), 104265.

[18] T. LIU, *A High-Resolution Method for Multi-Medium Compressible Flows and Its Applications*, PhD Thesis, 2001.

[19] P. H. MAIRE, R. ABGRALL, J. BREIL, R. LOUB'ERE, AND B. REBOURCET, *A nominally second-order cell centered Lagrangian scheme for simulating elastic-plastic flows on two-dimensional unstructured grids*, J. Comput. Phys. 235 (2013), 626-–665.

[20] G. H. MILLER, AND P. COLLELA, *A high-order Eulerian Godunov method for elastic-plastic flow in solids*, J. Comput. Phys. 167 (2001), 131—176.

[21] H. S. TANG, AND F. SOTIROPOULOS, *A second-order Godunov method for wave problems in coupled solid–water–gas systems*, J. Comput. Phys. 151(2) (1999), 790–815.

[22] J. A. TRANGENSTEIN, R. B. PEMBER, *Numerical algorithms for strong discontinuities in elastic-plastic solids*, J. Comput. Phys. 103(1) (1992), 63–89.

[23] M. L. WILKINS, *Calculation of Elastic-Plastic Flow* in: *Methods in Computational Physics, Vol. 3*, Academic Press (1964), 211–263.